






Glutamate dehydrogenase1 supports HIF-1 α stability to promote colorectal tumorigenesis under hypoxia

Kunhua Hu^{1,†} , Yufeng Ding^{2,†} , Hongwen Zhu^{3,†} , Xiaoqian Jing^{4,†}, Weiling He^{5,*}, Hua Yu^{2,**}  & Xiongjun Wang^{2,***} 

Abstract

Tumor cells surviving hypoxic stress acquire the ability to drive cancer progression. To explore the contribution of dehydrogenases to the low oxygen concentration response, we used siRNAs targeting 163 dehydrogenase-coding genes and discovered that glutamate dehydrogenase 1 (GDH1) plays a critical role in regulating colorectal cancer (CRC) cell survival under hypoxia. We observed that GDH1 deficiency had an inhibitory effect on CRC occurrence and impaired hypoxia-inducible factor 1- α (HIF-1 α) stability even under hypoxia. Mechanistically, hypoxia triggered p300 recruitment to GDH1, promoting its acetylation at K503 and K527. GDH1 acetylation at K527 induced the formation of a GDH1 complex with EGLN1/HIF-1 α ; in contrast, GDH1 acetylation at K503 reinforced its affinity for α -ketoglutarate (α KG), and glutamate production. In line with this view, α KG is a product of GDH1 under normoxia, but hypoxia stimulation reversed GDH1 enzyme activity and α KG consumption by the EGLN1/HIF-1 α complex, increasing HIF-1 α stability and promoting CRC progression. Clinically, hypoxia-modulated GDH1 AcK503/527 can be used as a biomarker of CRC progression and is a potential target for CRC treatment.

Keywords acetylation; colorectal cancer; GDH1; HIF1 α ; α -ketoglutarate

Subject Categories Cancer; Metabolism

DOI 10.15252/emboj.2022112675 | Received 25 September 2022 | Revised 15

March 2023 | Accepted 23 March 2023 | Published online 24 April 2023

The EMBO Journal (2023) 42: e112675

Introduction

When the stress signal of extracellular oxygen exhaustion is transduced to intracellular EGLN1, a process of stress called hypoxia

occurs. Tumor cells that survive hypoxia acquire the ability to metastasize, resist drugs, or tolerate nutrient limitation. However, how tumor cells survive in response to hypoxia is still unclear. Upon hypoxia, HIF1 α is reported to be stabilized and accumulated in various cancer cells and is associated with the progression and adverse clinical outcome of many different tumor types, including colorectal cancer (CRC) (Brahimi-Horn *et al*, 2007; Bögürçü *et al*, 2018). Hence, discovery of a potential strategy to modulate the tumor cell response to hypoxia would be of great significance.

The activity of EGLN1 is tightly associated with HIF1 α stability and is affected by the EGLN1 substrate oxygen and cofactor α KG. α KG is not only an intermediate metabolite in the Krebs cycle but also a direct product of glutamate metabolism (Stillman *et al*, 1993). Multiple enzymes are involved in α KG metabolism. For example, glutamic-oxaloacetate transaminase (GOT) and members of the glutamic-pyruvic transaminase (GPT) family produce α KG via glutamate deamination or a transaminase reaction. Members of the GDH family produce α KG via glutamate dehydrogenation, while members of the isocitrate dehydrogenase (IDH) family produce α KG via isocitrate dehydrogenation. In glioma cells, the absence of GDH1 was found to reduce the cellular level of α KG by approximately 65%, indicating that GDH1 might play a major role in α KG production in glioma cells (Yang *et al*, 2009). However, there is no clear association between α KG and CRC progression under hypoxia.

Generally, α KG is maintained at a steady state within the cell (Wang *et al*, 2019b), but dramatic changes in intracellular α KG levels profoundly impact gene transcription and signal transduction. Given that α KG is a cofactor for dioxygenases, such as TETs, KDMs, and EGLNs, it is reasonable to question whether changes in intracellular α KG levels can alter the activities of these enzymes. For example, the absence of BCAT1 was shown to cause α KG to accumulate to twice its basal level, and this increase in α KG activated EGLN1, which in turn inhibited the stability of HIF1 α (Raffel *et al*, 2017).

1 Guangdong Key Laboratory of Liver Disease Research, The Third Affiliated Hospital of Sun Yat-Sen University, Guangzhou, China

2 School of Life Sciences, Precise Genome Engineering Center, Guangzhou University, Guangzhou, China

3 Department of Analytical Chemistry and CAS Key Laboratory of Receptor Research, Shanghai Institute of Materia Medica, Chinese Academy of Sciences, Shanghai, China

4 Department of General Surgery, Ruijin Hospital, Shanghai Jiao Tong University School of Medicine, Shanghai, China

5 The First Affiliated Hospital of Sun Yat-Sen University, Guangzhou, China

*Corresponding author. Tel: +86-020-87755766; E-mail: hewling@mail.sysu.edu.cn

**Corresponding author. Tel: +86-020-86236055; E-mail: yuhua@sibcb.ac.cn

***Corresponding author. Tel: +86-020-86236055; E-mail: xiongjunwang@sibs.ac.cn; wangxiongjun@gzhu.edu.cn

†These authors contributed equally to this work

However, the K_m value of EGLN1 for α KG is 1.3 μ M (Lorenzo *et al*, 2014), and the intracellular α KG concentration varies from approximately 10–200 μ M depending on the cell context (Jin *et al*, 2015). Also, a prolyl hydroxylases *in vitro* assay showed 2-Hydroxyglutarate (2HG) could activate EGLN1 (Tarhonskaya *et al*, 2014) probably because 2HG has a similar structure with α KG and meanwhile *in vitro* assay facilitated the enriched 2HG to bind EGLN1. Therefore, we suspect that the global change in α KG concentration induced by BCAT1 or other α KG-producing or -consuming enzymes should be insufficient to affect the enzyme activity of EGLN1 by exchanging of α KG/2HG.

In this study, we found that once cells suffer hypoxia stress, GDH1 targets the EGLN1/HIF1 α complex after GDH1 acetylation by p300. In detail, AcK527 induced the formation of the GDH1/EGLN1/HIF1 α axis, while GDH1 acetylation at K503 alleviated the restriction of α KG binding to GDH1, AcK503-GDH1 resulted in glutamate production using α KG as substrate. As a consequence of the combined GDH1 acetylation at K503 and K527, the reversed GDH1 activity likely consumed α KG around the GDH1/EGLN1/HIF1 α complex, which led to the inhibition of EGLN1 activity and in turn stabilized HIF1 α . Of note, the synchronic acetylation of GDH1-K503/K527 can be used as a biomarker of CRC progression, and thus, blockade of AcK503/527-GDH1 would benefit CRC treatment.

Results

GDH1 is required for the response to hypoxia and is associated with a poor prognosis in CRC

To discover the contribution of tumor metabolism, especially dehydrogenases, to the hypoxia response, we screened 163 dehydrogenase-coding genes under hypoxia and observed that GDH1 depletion dramatically induced cell death under hypoxia (Fig 1A). We depleted GDH1 in HCT116 and SW480 cells (Fig EV1A) and found that CRC cells lacking GDH1 were more sensitive to hypoxia than those expressing GDH1, while loss of GDH1 slightly reduced cell proliferation under normoxic conditions (Fig EV1B). In addition, compared with the control cells, the percentage of apoptotic cells increased in the GDH1 depletion group, especially under hypoxia (Fig 1B and C). Supplementation with cell-permeable α KG was successfully executed (Fig EV1C), but the restored α KG did not rescue the effect on HIF1 α protein levels (Fig EV1D) and cell viability (Fig EV1E) in the cells lacking GDH1 under hypoxia, indicating that GDH1 might play an intricate role under hypoxia. Measurement of glutamate and ammonia levels reflects the possible conversion of GDH1 enzyme activity under normoxia and hypoxia because the increased glutamate and ammonia concentrations after GDH1 depletion under normoxia were consumed under hypoxia (Fig EV1F and G). Supplementation with octyl-2-hydroxyglutarate (2HG) also had no significant effect on HIF1 α protein stability, suggesting that globally increased 2HG does not efficiently compete with α KG for EGLN1 binding (Fig EV1H). Under hypoxia, HIF1 α protein levels in the control groups were higher than those in GDH1-depleted cells, while HIF2 α protein levels were slightly decreased after GDH1 depletion (Fig 1D). Compared with control cells, HIF1 α protein levels were higher in CRC cells overexpressing GDH1, and overexpression of GDH1 conferred CRC cell resistance to hypoxia and resulted in a

lower percentage of apoptotic cells *in vitro* and *in vivo* (Fig EV1I–L). The overall α KG content increased under hypoxia compared with normoxia. Loss of GDH1 impaired the increase in the overall α KG level under normoxia but not hypoxia. Consistent results were observed in cells overexpressing GDH1 under normoxia and hypoxia (Figs 1E and EV1M). These data suggest that GDH1 may not exhibit dehydrogenase activity under hypoxia.

Furthermore, we ruled out the effect of GDH1 on HIF1A transcription levels (Fig 1F), suggesting that GDH1-induced upregulation of the HIF1 α protein level is mainly achieved by facilitating the stabilization of HIF1 α under hypoxia rather than by affecting the level of gene transcription. The ability of CRC cells lacking GDH1 to form tumors also decreased drastically (Fig 1G and H). To examine GDH1 expression at the clinical level, we assessed the mRNA levels of GDH1 in 16 pairs of CRC and matched paracancerous samples and found that GDH1 did not exhibit high tumor tissue-specific expression (Fig 1I). In tumor tissues, we observed a positive correlation between the GDH1 and HIF1 α protein levels (Fig 1J).

Taken together, our primary data suggest that GDH1 participates in regulating HIF1 α stability, potentially offering a novel way to stabilize HIF1 α .

GDH1 depletion in the mouse intestine impairs CRC progression

To investigate the role of GDH1-mediated oncogenesis *in vivo*, we attempted to construct GDH1 knockout mice but found that mouse embryos showed serious defects and frequently died after GDH1 deletion. Therefore, tissue-specific knockout of GDH1 in the intestine was performed using the Cre-loxP recombination system and was verified by PCR, immunohistochemistry (IHC), and immunoblotting (Figs 2A and B, and EV2A).

The azoxymethane (AOM)/dextran sodium sulfate (DSS) model is a widely used inflammation-associated colon cancer model in rodents (De Robertis *et al*, 2011; Thaker *et al*, 2012). Loss of GDH1 in the intestine significantly reduced the occurrence of CRC in adult mice (Fig 2C). We also observed delayed appearance of tumors after depletion of GDH1 in the mouse intestine (Fig 2D). Furthermore, H&E staining verified the presence of tumors in the intestine (Fig 2E). Of note, equal infiltration of macrophages or microglial cells in the control and GDH1^{IEC-/-} mice was discovered by assessing approximate F4/80 positivity (Fig 2F), and no significant difference was found in the production of proinflammatory cytokines, such as TNF α , IL6, and IFN γ , after AOM/DSS induction in the control and GDH1^{IEC-/-} mice (Fig EV2B). However, focal regions of continuous ZO-1 staining were destroyed in control wild-type mice but remained relatively intact in GDH1-depleted mouse colons (Fig 2G). Mice without GDH1 in the intestine exhibited tolerance to AOM/DSS and a delayed decrease in body weight (Fig 2H). Consistently, GDH1 depletion significantly prolonged the survival time of mice after AOM/DSS treatment (Fig 2I). IHC of GDH1 and HIF1 α and H&E staining showed that GDH1 depletion in the intestine limited CRC development and HIF1 α levels (Fig 2J). Furthermore, HIF1 α protein was almost undetectable in GDH1^{IEC-/-} mice, whereas high levels of HIF1 α were found in the intestinal cancer tissues of WT mice treated with AOM/DSS (Fig 2K); however, no significant difference in HIF1A mRNA expression was observed in GDH1^{IEC-/-} and GDH1^{IEC+/+} mice without or with DSS treatment (Fig EV2C). Hence, GDH1 can promote intestinal cancer development, possibly by

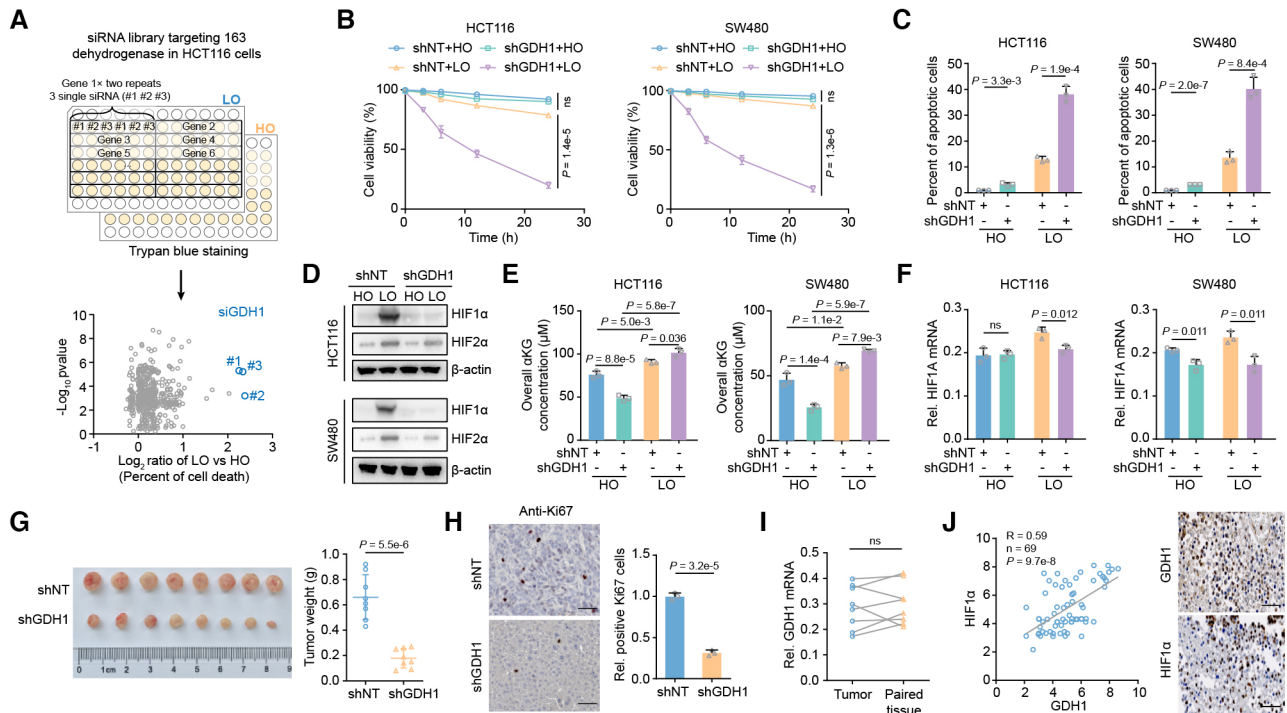


Figure 1. GDH1 confers tumor cell resistance to hypoxia and promotes tumorigenesis.

- A** The workflow for screening the dehydrogenase-coding genes required for resisting hypoxia in HCT116 cells. In detail, HCT116 cells were collected and plated in 96-well plates. Cells were transiently transfected with siRNAs separately targeting 163 dehydrogenase-coding genes identified in the KEGG database using RNAiMAX for 36 h, treated with or without hypoxia for 24 h, and finally stained with Trypan blue. The origin of siRNA library was released from horizondiscover website. The x-axis represents the \log_2 -transformed fold changes in the percentage of dead cells among LO- vs. HO-treated cells. Normoxia, 20% oxygen, is also termed HO. Hypoxia, 0.5% oxygen, is also termed LO.
- B** HCT116 and SW480 cells with GDH1 knockdown were incubated under normoxia and hypoxia, respectively. Then, cell viability was assessed by trypan blue staining ($n = 3$).
- C** The cells in (B) were collected after incubation under normoxia or hypoxia, and PI/Annexin V double staining was then used to measure the percentage of apoptotic cells via FACS ($n = 3$).
- D** The cells in (B) were collected after incubation under normoxia or hypoxia induction for 6 h, and the HIF1 α protein level was measured via immunoblot analysis.
- E** HCT116 and SW480 cells with GDH1 knockdown were incubated under normoxia and hypoxia, respectively. Then, overall α KG was assessed using an α KG assay kit (Abcam) ($n = 3$).
- F** HIF1A gene transcription was slightly impaired after GDH1 depletion. The cells in (B) were collected after incubation under normoxia or hypoxia, and the HIF1A mRNA level was analyzed via quantitative real-time PCR (qRT-PCR) ($n = 3$; ns, not significant).
- G, H** Tumor formation study. HCT116-shNT and HCT116-shGDH1 cells were injected into the left groin of nude mice. When the tumor size reached 300 mm³, the mice were sacrificed, and the tumors were removed for further experiments ($n = 8$) (G). Solid tumors were stained with an antibody against Ki67 (Scale bars: 50 μ m) ($n = 3$) (H).
- I** The relative mRNA level of GDH1 was determined in 8 paired CRC and adjacent tissues ($n = 8$).
- J** Positive correlation between GDH1 and HIF1 α protein expression in CRC tissue.

Data information: Data are mean \pm SD from the biological replicates (B, C, E–H). Statistics: two-way ANOVA with Tukey's HSD *post hoc* test (B); unpaired two-tailed student's *t*-test (C, F–H, J); one-way ANOVA followed by with Tukey's HSD *post hoc* test (E); paired two-tailed Student's *t*-test (I). Source data are available online for this figure.

increasing HIF1 α stability once hypoxia occurs during CRC progression.

Hypoxia-induced acetylation of GDH1 is required for HIF1 α stability

To explore the correlation between GDH1 and HIF1 α stability, we first excluded the possibility that hypoxia could affect GDH1 protein levels in CRC cells (Fig 3A). Then, we inserted a FLAG tag into the GDH1 C-terminus, which had no effect on GDH1 activity (Fig EV3A and B). Using this system, we enriched GDH1 and observed decreased GDH1 dehydrogenase activity under hypoxia (Fig 3B).

Under hypoxia, the level of GDH1 panlysine (K) acetylation, but not K methylation and S/T/Y phosphorylation, was significantly increased (Fig 3C), suggesting that GDH1 lysine acetylation is involved in the hypoxia response. The enriched GDH1-FLAG was identified by liquid chromatography–mass spectrometry (LC–MS). GDH1 acetylation sites at K503 and K527 were detected under hypoxia but not under normoxia (Fig EV3C and D). Both the mutations of K503 to R503 and K527 to R527 impaired GDH1 acetylation under hypoxia. When these two lysine sites were simultaneously mutated to arginine residues, GDH1 acetylation was heavily impaired (Fig 3D and E). Furthermore, after mutation of K503 and K527 to R503 and R527, respectively, the transcriptional activity of HIF1 α

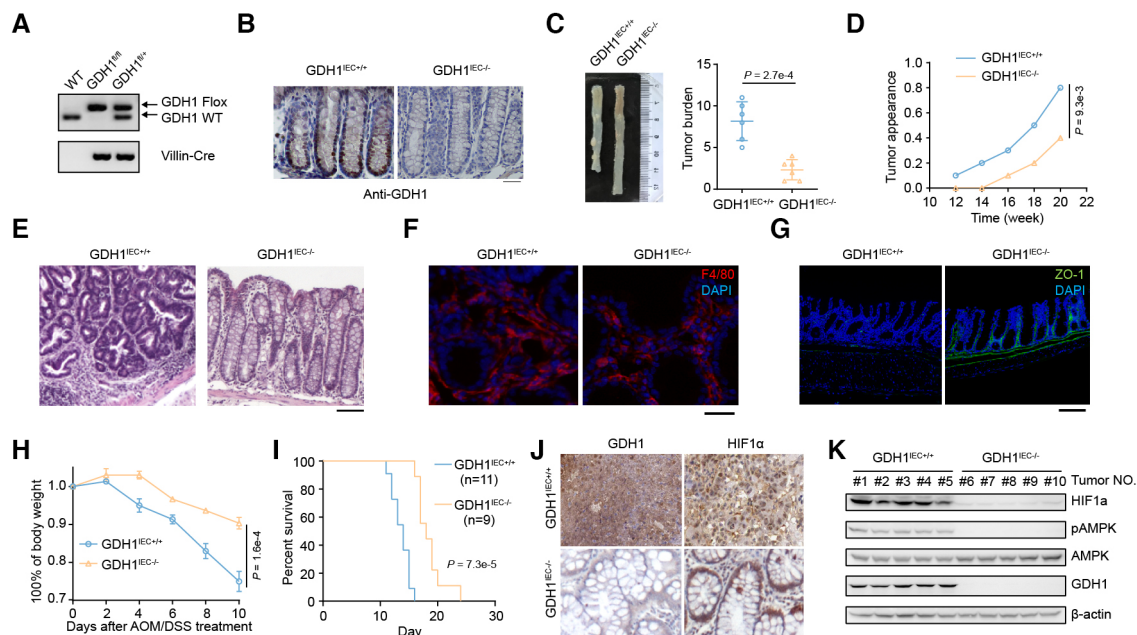


Figure 2. Depletion of GDH1 in the mouse intestine impairs colorectal cancer formation.

- A Identification of GDH1 knockout (KO) in mouse intestines by PCR.
 B Identification of GDH1 KO in mouse intestines by immunohistochemistry (IHC).
 C–E The AOM/DSS-induced inflammatory cancer switch was reduced by the loss of GDH1. (C) Tumor burden ($n = 6$). (D) Tumor appearance. (E) H&E staining of colon cancer tumors from GDH1^{IEC+/+} and GDH1^{IEC-/-} mice (scale bar, 200 μ m).
 F F4/80 staining in a noninflamed portion of the colon after AOM/DSS treatment (scale bar, 50 μ m).
 G ZO-1 staining in colon sections of mice treated with sequential AOM/DSS treatment (scale bar, 200 μ m).
 H Body weight of GDH1^{IEC+/+} and GDH1^{IEC-/-} mice after AOM/DSS treatment ($n = 3$).
 I Survival percentages of GDH1^{IEC+/+} mice ($n = 11$) and GDH1^{IEC-/-} mice ($n = 9$) during progression of the inflammatory cancer switch.
 J GDH1 and HIF1 α protein expression in CRC tissue from GDH1^{IEC+/+} mice and GDH1^{IEC-/-} mice.
 K Both HIF1 α protein levels and AMPK activity were assessed in the intestine of GDH1^{IEC-/-} mice after AOM/DSS treatment using the indicated antibodies.

Data information: Data are mean \pm SD from the biological replicates (C, H). Statistics: unpaired two-tailed Student's *t*-test (C); two-way ANOVA with Tukey's HSD *post hoc* test (D, H); log-rank test (I).

Source data are available online for this figure.

decreased by approximately 75% (Fig 3F). Meanwhile, the protein levels of HIF1 α under hypoxia decreased by more than half after the loss of GDH1 acetylation at K503 or K527 (Fig 3G).

The data showed delayed and weak stabilization of HIF1 α protein levels when K503/527 was mutated to R503/527, offering solid evidence that the protein stability of HIF1 α is regulated by GDH1 lysine acetylation (Fig 3H and I). Based on these data, we preliminarily ascertained that hypoxia-induced acetylation of GDH1 is required for HIF1 α stability.

Hypoxia-induced GDH1 acetylation at K503 reverses GDH1 dehydrogenase activity

How does hypoxia-mediated GDH1 acetylation modulate the protein stability of HIF1 α ? As shown in Fig 4A and B, GDH1 with the K503R mutation increased the formation of GDH1 hexamers compared with WT GDH1. K527R-GDH1 polymer formation was more or less consistent with that of WT-GDH1 (Fig 4A and B). Hence, we speculated that GDH1 acetylation at K503 regulates GDH1 dehydrogenase activity.

Consistent with this speculation, upon hypoxia stimulation, the relative level of α KG produced by K503R-GDH1 was

significantly increased while The K527R mutation did not affect GDH1 enzyme activity (Fig 4C). However, compared with that of WT-GDH1, the ability of K503R-GDH1 to produce α KG was reduced by around 50%, while the ability of the K503Q-GDH1 mutant to produce glutamate was increased by approximately 130% (Figs EV4A and 4D). In line with the above *in vitro* assay, the relative intracellular α KG content decreased in cells expressing the K503Q mutant, while that in cells expressing the K503R mutant increased under hypoxia compared with that in control cells (Figs EV4B and 4E).

The results of an enzyme kinetics experiment showed that K503Q-GDH1 had a much lower maximum reaction rate (V_{max}) of α KG production than GDH1-WT, whereas K503R-GDH1 had a moderately higher V_{max} of α KG production than GDH1-WT, suggesting that K503Q-GDH1 has a heavily impaired ability to use glutamate (Glu) as a substrate (Fig 4F). To exclude the possibility that the K to Q mutation does not effectively mimic acetylation modification, we also purified AcK503-GDH1, K503Q-GDH1, and K503R expressed in *E. coli* (Fig EV4C). The qualities and activities of the above proteins were ascertained by a series of *in vitro* experiments, such as LC-MS for modification identification, FPLC and dynamic light scattering

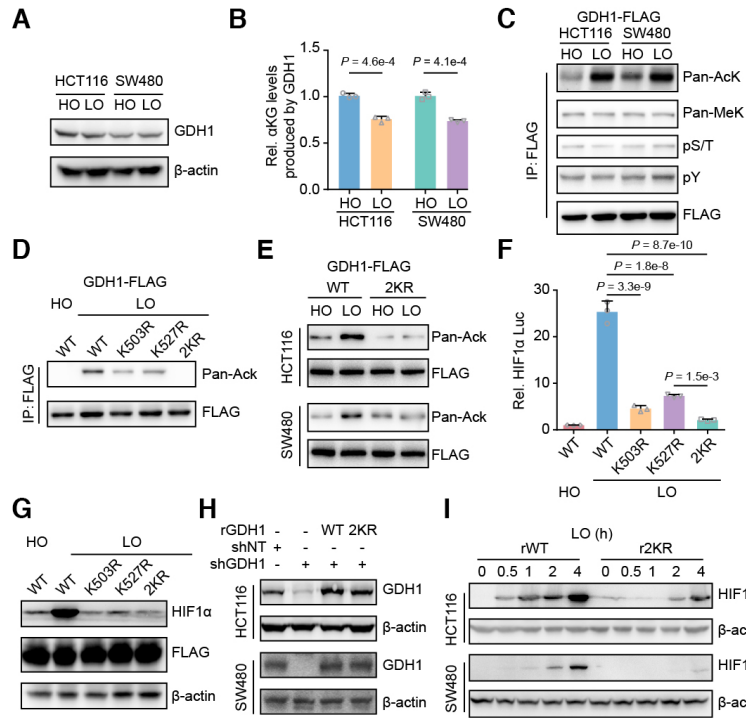


Figure 3. Hypoxia-induced GDH1 acetylation was required for HIF1 α stability.

- A HCT116 and SW480 cells were incubated under normoxia and hypoxia, respectively. Then, the cells were collected, and the GDH1 protein level was analyzed via immunoblotting.
- B Hypoxia reduced the activity of GDH1 in producing α KG. A FLAG tag was inserted into the GDH1 C-terminus in HCT116 and SW480 cells. The cells were collected after incubation under normoxia or hypoxia, and M2 flag beads were used to enrich FLAG-tagged GDH1. GDH1-FLAG was used to assess the enzymatic activity of GDH1 in producing α KG ($n = 3$).
- C GDH1-FLAG in (B) was examined using antibodies against pan-lysine acetylation and methylation and pan-serine/threonine and tyrosine phosphorylation.
- D GDH1 acetylated at both K503 and K527 under hypoxia. K503R and K527R were mutated endogenously. GDH1-FLAG was enriched, and an antibody against pan-lysine acetylation was used to examine lysine acetylation of GDH1 when K503 or K527 was mutated to R503 or R527. 2KR represents K503/K527R.
- E HCT116 or SW480 cells containing WT or GDH1 with K503/K527R mutations were incubated under normoxia and hypoxia, respectively. GDH1-FLAG was enriched, and an antibody against pan-lysine acetylation was used to test GDH1-lysine acetylation.
- F Loss of acetylation at GDH1-K503 or GDH1-K527 impaired the transcriptional activity of HIF1 α ($n = 3$).
- G HIF1 α protein stability under hypoxia depends on GDH1-K503 and GDH1-K527 acetylation.
- H GDH1-depleted cell lines were constructed and then rescued with the expression of wild-type GDH1 or K503/K527R mutant GDH1.
- I HIF1 α protein stability in rWT or r2KR mutant cells was induced over time under hypoxia.

Data information: Data are mean \pm SD from the biological replicates (B, F). Statistics: unpaired two-tailed Student's *t*-test (B); one-way ANOVA with Tukey's HSD *post hoc* test (F).

Source data are available online for this figure.

(DLC) to determine dimerization and NADH measurement to assess GDH1 dehydrogenase activity (Fig EV4D–G). AcK503-GDH1 had a V_{max} of α KG or Glu production similar to that of K503Q-GDH1, demonstrating that the K503Q mutant mimics acetylation at K503 (Fig 4G). Moreover, we experimentally defined the Michaelis–Menten constant (K_m) value of these GDH1 variants for Glu. The calculated K_m value indicated that K503Q-GDH1 had a much lower Glu affinity than GDH1-WT, whereas K503R-GDH1 had a higher Glu affinity than GDH1-WT (Fig 4H). Isothermal titration calorimetry (ITC) further showed that AcK503- and K503Q-GDH1 showed increased GDH1 to α KG binding affinity compared with WT or K503R-GDH1, which was consistent with the results of previous enzyme assays in which the K503Q mutation reduced the ability of GDH1 to produce α KG (Fig 4I). We also summarized the effect of K503 acetylation on the exchange of the GDH1 trimer and hexamer, which indicates the conversion of GDH1 activity (Fig 4J).

Notably, the K503Q mutation reduced the binding affinity of Glu to GDH1 but had no effect on NAD^+ binding to GDH1 (Fig EV4H and I). Molecular simulation revealed that GDH1-His (H) 266, -H507 and GTP form a hydrogen bond network and that hypoxia-induced acetylation at K503 of GDH1 locks GTP in the hydrogen bond network of H266-H507, in turn reinforcing α KG in GDH1 as a substrate. Otherwise, the position of K527 is located in a large flat groove and facilitates GDH1 association with other partner proteins (Fig EV4J). Thus, we preliminarily conclude that under hypoxia, GDH1 enzyme activity is reversed by acetylation at K503.

Hypoxia-induced GDH1 acetylation at K527 anchors GDH1 to the EGLN1/HIF1 α complex

To find the correlation between HIF1 α stability and the overall α KG content, we overexpressed certain enzymes that produce or

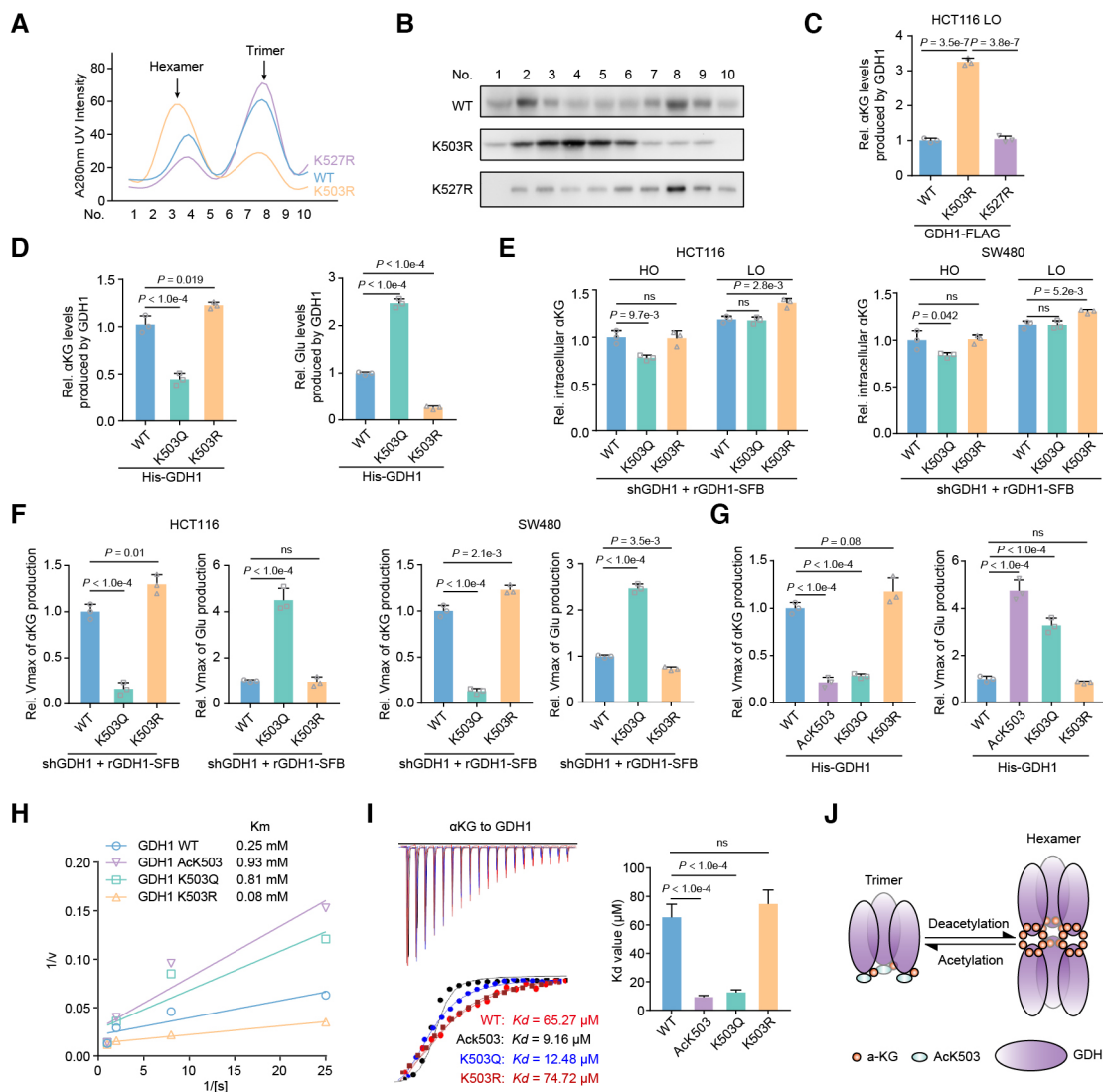


Figure 4. GDH1 acetylation at K503 reverses GDH1 dehydrogenase activity through decreased formation of GDH1 hexamers.

- A** GDH1-FLAG (including WT and K503R and K527R mutants) was enriched and analyzed via fast protein liquid chromatography (FPLC).
B Immunoblot analysis of GDH1-FLAG levels at different time points.
C The K503R mutation enhances GDH1 activity in producing α KG. FLAG-tagged GDH1 was purified from HCT116 cells ($n = 3$).
D The K503Q mutation reduces GDH1 activity leading to α KG production while enhancing the enzymatic activity leading to Glu production. His-tagged GDH1 was purified from *E. coli* ($n = 3$).
E, F HCT116 or SW480 cells were depleted of endogenous GDH1 and rescued with SFB-tagged rGDH1 WT, K503Q or K503R. The relative intracellular α KG concentration was measured under normoxia and hypoxia (**E**). rGDH1-SFB proteins were enriched using M2-FLAG beads to determine the Vmax of α KG production (**F**) ($n = 3$).
G–I His-GDH1 proteins (including WT, AcK503, K503Q and K503R) were purified from *E. coli* to determine the Vmax of α KG and Glu production (**G**). A Lineweaver–Burk plot was used to determine the Michaelis–Menten constant (K_m) value for Glu production by the GDH1 proteins (**H**) ($n = 3$). ITC assays were performed with precipitated His-GDH1 proteins and α KG (**I**) ($n = 3$).
J Cartoon illustrating the working mechanism of the GDH1 acetylation-mediated decrease in hexamers and the enhanced binding affinity to α KG.

Data information: Data are mean \pm SD from the biological replicates (C–G, I). Statistics: one-way ANOVA with Tukey's HSD *post hoc* test (C–G, I).

Source data are available online for this figure.

consume α KG, and we observed that HIF1 α protein was not regulated by global changes in α KG (Fig 5A and B). Furthermore, to elucidate the mechanism by which GDH1 mediates HIF1 α protein stability, we applied liquid chromatography coupled with tandem mass spectrometry (LC–MS/MS) to verify both HIF1 α and EGLN1 as GDH1-interacting proteins under hypoxia (Fig 5C). Reverse Co-IP

was performed to test whether EGLN1 interacts with other α KG producers or consumers, such as BCAT1/2, GOT1/2, IDH1/2, and GPT (Fig EV5A). Using fraction assays and immunofluorescence (IF) experiments, we clarified that GDH1 interacts and colocalizes with EGLN1 in the cytosol upon hypoxia (Fig 5D and E). Under hypoxia, GDH1 accumulated in the cytosol but showed a slightly decreased

Figure 5. Tumor cells require both GDH1-K503 and GDH1-K527 acetylation to simultaneously reduce EGLN1 activity under hypoxia.

- A, B Immunoblot of the HIF1 α protein level under hypoxia for 6 h when enzymes related to the α KG level were overexpressed in cells, including GDH1 (A). Relative α KG levels in contrast to the control (B) ($n = 3$).
- C HCT116-GDH1-FLAG cells were incubated under normoxia and hypoxia. Cells were then collected, and M2 flag beads were used to enrich FLAG-tagged GDH1. GDH1-FLAG-associated proteins were identified by LC-MS/MS. The fold change was evaluated as the ratio of expression under hypoxia to that under normoxia. The x-axis represents the \log_2 -transformed fold change, and the y-axis represents the minus \log_{10} -transformed P -value.
- D A Co-IP assay was performed to test the interaction between GDH1 and EGLN1 in the cytosolic and mitochondrial fractions from HCT116-GDH1-FLAG cells.
- E Immunofluorescence analysis of GDH1-FLAG and HA-EGLN1 was performed to assess their colocalization under normoxia and hypoxia.
- F GDH1-FLAG was enriched in the cytosolic and mitochondrial fractions from HCT116-GDH1-FLAG cells, and the enzymatic activity of GDH1 in producing α KG was evaluated ($n = 3$).
- G HCT116 cells were cotransfected with plasmids encoding GDH1-FLAG and HA-EGLN1. A Co-IP assay was performed to examine whether the K503R or K527R mutation affected the interaction between GDH1 and EGLN1.
- H, I EGLN1 activity test. After hypoxia stimulation for 1 h, HA-EGLN1 was enriched in HCT116-shGDH1 cells restored with WT or mutant GDH1 (H). His-GDH1 with K503 or K527 acetylation (AcK503 or AcK527) and mimic acetylation at K503 or K527 (K503Q or K527Q) were purified from *E. coli*. Then, His-GDH1 was incubated for 1 h with HA-EGLN1 (I). EGLN1 activity was tested by converting α KG to succinate ($n = 3$).
- J, K Relative α KG content in EGLN1. HA-EGLN1 was enriched in shNT or shGDH1 cells under hypoxia. A radiometric ^{14}C - α KG-EGLN1 binding assay was performed using HA-EGLN1 incubated with ^{14}C - α KG (J). Alternatively, the HA-EGLN1 protein was digested by trypsin, and α KG was determined by LC-MS/MS analysis (K) ($n = 3$).
- L–N Detection of HIF1 α protein stability (L); the mRNA expression levels of the HIF1 α target genes GLUT1, HK1, PGK1 and CCND1 (M); and HIF1 α transactivation (N) in the indicated cell lines under hypoxia ($n = 3$).
- O Detection of HIF1 α protein stability in the indicated cell lines under normoxia.
- P HIF1 α transactivation was examined in the indicated cell lines under hypoxia with or without treatment with the HIF1 α transactivation inhibitor 2-MeOE2 (1 μM) for 12 h ($n = 3$).

Data information: Data are mean \pm SD from the biological replicates (B, F, H–K, M, N, P). Statistics: one-way ANOVA with Tukey's HSD *post hoc* test (B, F, H–K, M, N, P); unpaired two-tailed Student's t -test (C).

Source data are available online for this figure.

presence in mitochondria. More importantly, cytosolic GDH1 presented lower dehydrogenase activity (Fig 5F). Furthermore, we performed a Co-IP assay and found that loss of GDH1 acetylation at K527 abolished the interaction between GDH1 and EGLN1 (Fig 5G). Mimicked acetylation at K503 or K527 reduced EGLN1 hydroxylase activity, while the loss of acetylation at K503 or K527 dramatically enhanced EGLN1 hydroxylase activity even under hypoxia (Fig 5H). We purified GDH1 with lysine acetylation or with mimicked acetylation expressed in *E. coli* or HCT116 cells, respectively, and then tested whether antibodies specifically targeted the corresponding lysine acetylation (Fig 5V5B). By incubating the above purified GDH1 proteins with EGLN1, we found that GDH1 acetylation at K503 but not at K527 constrained EGLN1 hydroxylase activity (Fig 5I). A potential explanation for this result is that GDH1 combined with EGLN1 in this *in vitro* reaction system and the effect of K527 acetylation was not reflected. As hypoxia drives GDH1 acetylation and targets EGLN1, the overexpression of WT-GDH1 dramatically impaired EGLN1 activity upon hypoxia (Fig 5V5C).

To test whether EGLN1-bound α KG is regulated by GDH1 acetylation at K503 or K527, we developed a radiometric ^{14}C - α KG-EGLN1 binding assay and LC-MS-based protein-bound metabolite assay. The consistent results of these two assays confirmed that acetylation at the K503 and K527 sites is indispensable for reducing the possibility of α KG binding to EGLN1 under hypoxia (Fig 5J and K). The specificity of the above assays to measure EGLN1-bound α KG was confirmed using an EGLN1 R383/398A mutant, which lost the ability to capture α KG, and we observed a competitive effect of WT-GDH1 overexpression on EGLN1-bound α KG (Fig 5V5D and E). Otherwise, EGLN1 activity was reduced in K503Q-GDH1 cells (Fig 5V5F). The acetylation of GDH1 at K503 or K527 is essential for maintenance of the stability of HIF1 α under hypoxia. In detail, the individual K503R and K527R mutations resulted in HIF1 α instability, and the 2KR double mutation reinforced this effect (Fig 5L). The expression of the HIF1 α downstream genes GLUT1, HK1, PGK1, and

CCND1 (Semenza, 2003; Luo *et al.*, 2006) was also significantly reduced when GDH1 deacetylation occurred or was mimicked (Figs 5M and 5V5G). In line with this, HIF1 α transactivation was impaired by deacetylation at K503 or K527, and this impairment was reinforced by the 2KR mutant in GDH1 (Fig 5N). Simultaneously, mutating K503 and K527 to mimic constitutive acetylation significantly enhanced the stability of HIF1 α under normoxia (Fig 5O). The increased HIF1 α stability induced by GDH1 acetylation at K503 and K527 was abolished by the HIF1 α transactivation inhibitor 2-MeOE2 (Fig 5P).

We also assessed the effect of individual mimic acetylation mutations on HIF1 α and found that mimic acetylation at K503 or K527 alone did not have a sufficient capacity to stabilize HIF1 α under hypoxia (Fig 5V5H) by exhausting α KG in EGLN1 (Fig 5V5I and J) and impaired EGLN1 activity (Fig 5V5K and L). Finally, the individual mimic acetylation mutations in GDH1 did not drive gene expression mediated by HIF1 α (Fig 5V5M).

Hence, upon hypoxia exposure, GDH1-K527 acetylation targets EGLN1, while GDH1-K503 acetylation produces glutamate using α KG as a substrate. The conversion of GDH1 enzyme activity prompts HIF1 α stability by consuming α KG in the GDH1/EGLN1/HIF1 α axis.

p300 acetylates GDH1 in cytosol

Using the K503R-GDH1 or K527R-GDH1 mutant to exclude nonspecific recognition, both antibodies were found to specifically identify GDH1 acetylation under hypoxia (Fig 6A) and indicated that the extent of AcK503 and AcK527 increased with prolonged hypoxia treatment time (Fig 6B). GDH1-AcK503 and GDH1-AcK527 were present in both the cytosol and nucleus (Fig 6C).

TIP60, PCAF, CBP, and p300 are four major acetyltransferases responsible for lysine acetylation (Wapenaar & Dekker, 2016). The knockdown efficiency of small interfering RNAs specifically

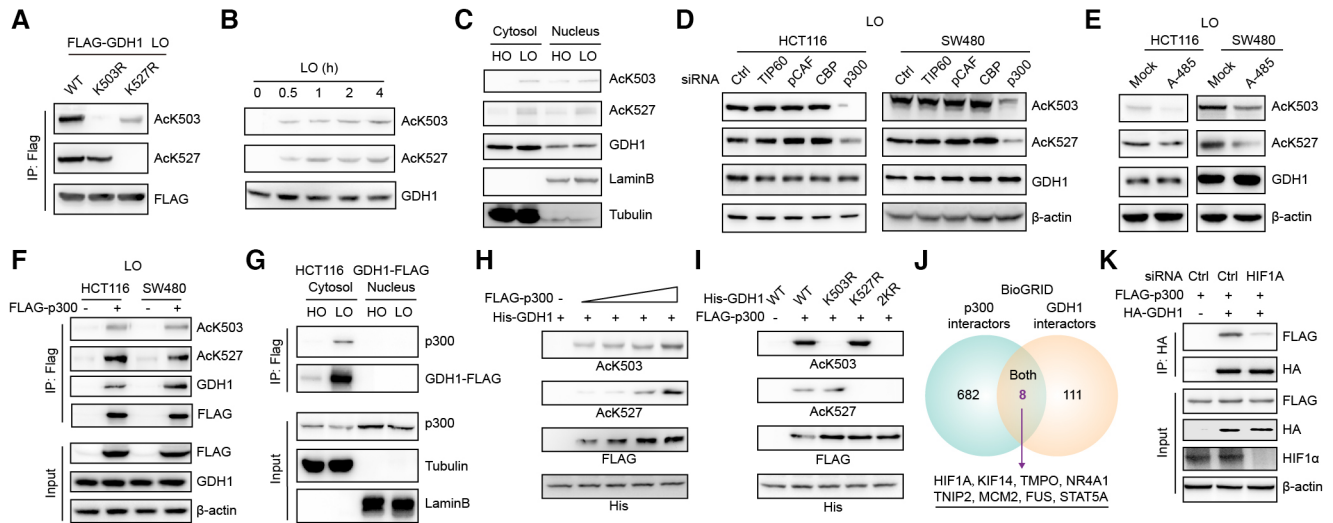


Figure 6. p300 acetylates GDH1 at K503 and K527 under hypoxia.

- A Immunoblot analysis identified the specificity of the antibody against GDH1-K503 or GDH1-K527 acetylation.
- B GDH1-K503 or GDH1-K527 acetylation increased with the time course of hypoxic stress.
- C GDH1-K503 or GDH1-K527 acetylation occurred in both the cytosol and nucleus.
- D, E The levels of both AcK503 and AcK527 were analyzed when cells were transfected with small interfering RNA (siRNA) targeting TIP60, PCAF, CBP or p300 (D) or when HCT116 or SW480 cells were treated with the p300 inhibitor A-485 (1 μ M) for 12 h under hypoxia (E).
- F HCT116 and SW480 cells were transfected with or without FLAG-p300. The p300-associated proteins were enriched with M2-FLAG beads and subjected to immunoblot analysis using antibodies against GDH1, GDH1-K503 or GDH1-K527 acetylation.
- G A Co-IP assay was performed to examine the interaction between GDH1 and p300 in the cytosolic and nuclear fractions of HCT116 GDH1-FLAG cells.
- H p300 acetylated GDH1 at K503 and K527 in a dose-dependent manner.
- I p300 specifically acetylates GDH1 at K503 and K527.
- J The GDH1 and p300 interacting proteins were extracted from the BioGRID database, and the shared interacting proteins are shown in a Venn diagram.
- K The HIF1A gene was transiently knocked down, and HCT116 cells were cotransfected with FLAG-p300 and HA-GDH1 for a Co-IP assay.

Source data are available online for this figure.

targeting the genes encoding the above acetyltransferases is shown in Appendix Fig S1A. p300 depletion induced a decrease in AcK503 and AcK527, while the knockdown of the other acetyltransferases did not have this effect (Fig 6D). Furthermore, using an inhibitor specifically targeting p300, we observed a result consistent with that obtained by p300 depletion with specific siRNA (Fig 6E). Co-IP experiments showed that the FLAG-p300-associated complex contained GDH1 acetylated at K503 and K527 (Fig 6F). Co-IP analyses of cytosolic and nuclear fractions identified GDH1 and p300 interacting in the cytosol but not in nuclei, suggesting that nuclear AcK503-GDH1 and AcK527-GDH1 first occurred in the cytoplasm (Fig 6G). As shown in the BioGRID database, approximately 30% of p300 interactors are localized in the cytosol (Appendix Fig S1B), and IF staining using an antibody against p300 showed that p300 localized in both the cytosol and nucleus (Appendix Fig S1C). Moreover, the HIF1 α protein level was blocked by p300 knockdown in WT-GDH1-overexpressing cells but not in 2KQ-GDH1-overexpressing cells (Appendix Fig S1D). These results demonstrate that p300 is required for GDH1 acetylation.

We also performed a semi-*in vitro* biochemical experiment in which gradually increased FLAG-p300 purified from HCT116 cells was incubated with His-GDH1 purified from *E. coli*, and the levels of AcK503-GDH1 and AcK527-GDH1 increased in this *in vitro* acetylation reaction system (Fig 6H). When we mutated K503 to R503 or K527 to R527, no signals for GDH1 acetylated at K503 or K527 were

detected, even when p300 was added to the acetylation reaction system (Fig 6I). To clarify how GDH1 recruits p300, we evaluated the common interacting proteins of GDH1 and p300 in the BioGRID database. As shown in Fig 6J, eight proteins, including HIF1 α , were potential bridges linking p300 to GDH1. We first transiently knocked down the HIF1A gene and found that HIF1A depletion resulted in an obvious reduction in the interaction between GDH1 and p300 (Fig 6K). The above results further confirm that p300 forms an axis with GDH1/HIF1 α and is responsible for acetylating GDH1 at K503 and K527.

GDH1 acetylation at both K503 and K527 is required to form solid tumors and is correlated with a poor CRC prognosis

Under hypoxia, the expression of the individual GDH1 K503R or GDH1 K527R mutant sensitized cells to hypoxia, and the GDH1 2KR mutant reinforced this effect (Fig 7A and Appendix Fig S2A). Consistently, only approximately 7% of 2KQ-GDH1 mutant cells were apoptotic. Under the same conditions, more than 30% of K503R-, K527R- or 2KR-GDH1 mutant cells were apoptotic (Fig 7B, Appendix Fig S2B and C). Moreover, HIF1 α knockdown blocked the increased resistance to apoptosis of WT or 2KQ-GDH1 cells under hypoxia but not of GDH1 knockdown cells, further supporting the existence of the GDH1/EGLN1/HIF1 α axis (Appendix Fig S2D). Experiments in tumor-bearing nude mice showed that GDH1 acetylation was

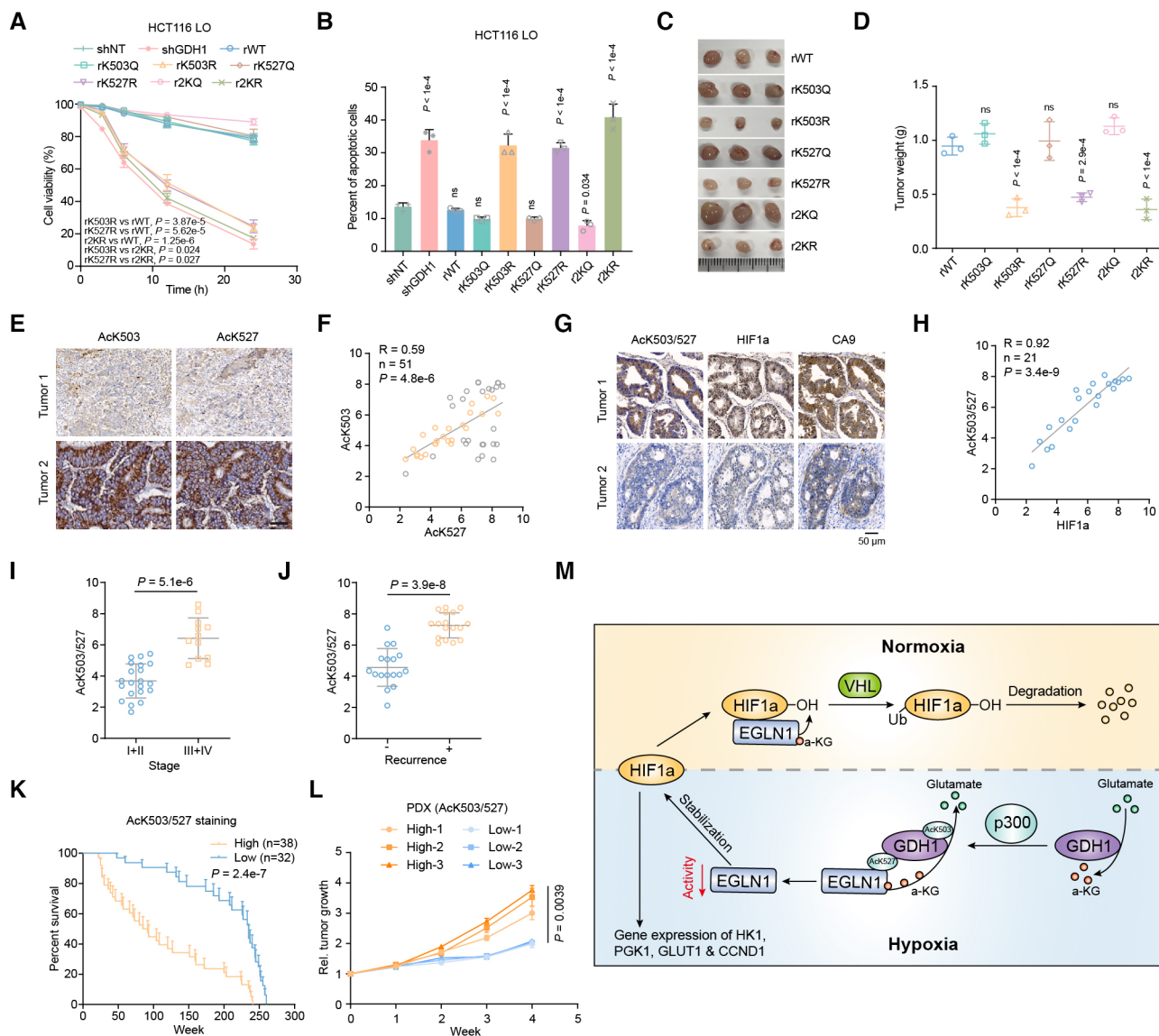


Figure 7. Ack503/527-GDH1 indicates a poor prognosis, mainly dependent on HIF1α stabilization.

A, B Cell viability and percentage of apoptosis in the indicated cell lines under hypoxia were analyzed by trypan blue (A) and PI/Annexin V double staining (B), respectively ($n = 3$).

C, D The xenograft tumor formation efficiency of the indicated cell lines was assessed, and tumor weight measurements were performed ($n = 3$).

E Representative images of CRC samples are shown after antibody staining of Ack503-GDH1 and Ack527-GDH1.

F The correlation between Ack503-GDH1 and Ack527-GDH1 expression in CRC samples. The tissue sections were quantitatively scored according to the percentage of positive cells and the staining intensity (H -score) ($n = 51$).

G Representative images of the same CRC samples are shown after staining with antibodies against Ack503/527-GDH1 and HIF1α.

H Correlation between Ack503/527-GDH1 and HIF1α expression in CRC samples ($n = 21$).

I Detection of Ack503/527-GDH1 expression in CRC grades I + II and III + IV (grade I + II, $n = 21$; grade III + IV, $n = 12$).

J Detection of Ack503/527-GDH1 expression in patients with (+) or without (-) recurrence (-, $n = 17$; +, $n = 17$).

K Patient survival corresponding to different levels of Ack503/527-GDH1 expression (High, $n = 38$; Low, $n = 32$).

L PDX growth related to high or low levels of Ack503/527-GDH1 expression.

M Schematic model described in the discussion section.

Data information: Data are mean \pm SD from the biological replicates (A, B, D, I, J, L). Statistics: two-way ANOVA with Tukey's HSD *post hoc* test (A, L); one-way ANOVA with Tukey's HSD *post hoc* test (B, D); unpaired two-tailed Student's *t*-test (F, H); Mann-Whitney *U*-test (I, J); log-rank test (K). Source data are available online for this figure.

required for the formation of solid tumors. A lack of GDH1 acetylation at K503 or K527 significantly decreased the ability of cells to form solid tumors (Fig 7C and D).

Because the simultaneous acetylation of GDH1 at K503 and K527 is required to maintain HIF1α stability, we first examined the correlation between Ack503 and Ack527 and then selected samples in

which AcK503 and AcK527 were highly positively correlated for subsequent experiments (Appendix Fig S2E, Fig 7E and F). To investigate the correlation between AcK503/527-GDH1 and HIF1 α at the tissue level, we prepared an antibody against AcK503/527-GDH1 by mixing the two acetylated peptides (Appendix Fig S2F–H). The AcK503/527-GDH1 and HIF1 α signals in tissues were highly positively correlated, indicating that HIF1 α protein stability is upregulated when GDH1 is diacetylated at K503/527 in the clinic (Fig 7G and H). The tumor tissue from AOM/DSS mice also presented a similar correlation between AcK503/527-GDH1 and HIF1 α in hypoxic regions (Appendix Fig S2I). The above experiments revealed that AcK503-GDH1/K527 is positively correlated with the degree of CRC malignancy (Fig 7I and J) and is expected to be a biomarker to characterize CRC progression and prognosis. Furthermore, we calculated the survival duration of patients in the two groups depending on their level of acetylated K503/K527-GDH1. Patients with high AcK503/527-GDH1 expression clearly presented a shorter survival time than those with low expression (Fig 7K). We observed a higher tumor growth rate in patient-derived xenografts (PDXs) from patients with a high AcK503/527-GDH1 expression (Fig 7L). The above data suggest that GDH1 acetylation at K503/K527 can indicate CRC progression under hypoxia.

Discussion

In this study, through siRNA screening targeting 163 dehydrogenase-coding genes, we found that GDH1 could confer tolerance to hypoxia. The effects of metabolic enzyme defects on organ development and pathology have been poorly studied. Using the Cre-loxP recombination system to selectively deplete metabolic enzymes in specific organs, we obtained a mouse model lacking the GDH1 gene in the small intestine. Although GDH1 knockout had no significant effect on intestinal development, AOM/DSS treatment did not effectively induce CRC in mice with GDH1 deletion in the intestine. Hence, first, through a series of *in vitro* and *in vivo* experiments, we ascertained the oncogenic role of GDH1 in CRC development by adapting tumor cells to hypoxic stress.

The formation of blood vessels occurs later in the process of solid tumor formation, which subjects solid tumors to many stresses, such as hypoxia and nutrient limitation (Hanahan & Weinberg, 2011). Solid tumors have developed strategies to address these stresses and survive. Here, we examined the stress response signaling pathways associated with hypoxia and nutrient limitation. AMPK phosphorylation and HIF1 α levels were significantly lower in CRC tissues of GDH1-deficient mice than in those of WT mice. We previously reported that GDH1 regulates AMPK phosphorylation under glucose deficiency (Wang et al, 2019a). In the present study, we found that GDH1 also plays a role in modulating HIF1 α stability. HIF1 α regulates a wide range of target genes involved in tumor cell growth, such as GLUT1, HK1, PGK1, and CCND1 (Semenza, 2003). Consequently, the expression of these genes was significantly decreased in GDH1-deficient CRC cells.

In both cell lines and animal models, we preliminarily verified that GDH1 is required to stabilize HIF1 α under hypoxia. In different cellular contexts, GDH1 depletion results in a 25–60% decrease in intracellular α KG levels (Yang et al, 2009; Jin et al, 2015). Given that α KG is a cofactor for members of the TET, DNMT, and EGLN

families, it is reasonable to hypothesize that changes in the level of α KG would alter the activity of these enzymes. EGLN family depends on multiple substrates and cofactors for activity, including α KG, 2HG, and iron availability, and on the presence of oxidative stress (Ke & Costa, 2006; Kaelin & Ratcliffe, 2008). It is reported that EGLN1 activity is not only regulated by oxygen but also regulated by the intracellular metabolite α KG, which competes with its analogue 2HG. For example, BCAT1 is reported to restrict α KG levels and thus promote glioma occurrence and survival by decreasing EGLN1 enzyme activity and increasing HIF1 α protein stability (Raffel et al, 2017); therefore, a correlation between BCAT1 and EGLN1 can be proposed. However, biochemistry indicators were not examined in their study. In fact, the *K_m* value of EGLN1 for α KG is 1.3 μ M (Lorenzo et al, 2014), while in different cell contexts, the intracellular α KG concentration changed in the range of 10–200 μ M, which was insufficient to affect EGLN1 enzyme activity. Meanwhile, although 2HG is a well-established competitive inhibitor of α KG, the global increase in 2HG induced by supplementation with cell-permeable octyl-2HG had no effects on EGLN1 activity in this study. This result was supported by a previous report showing that the IDH1-R132H mutant utilized α KG as a substrate and produced R-2HG, which did not stabilize HIF1 α protein (Koivunen et al, 2012). Conversely, forced expression of an IDH1-R132H mutant reduced α KG but increases HIF1 α protein (Zhao et al, 2009). The inconsistent results of the above studies suggest that global changes in intracellular α KG or 2HG do not uniformly affect EGLN1 activity. Thus, we should shift our perspective toward signal transduction-mediated local changes in α KG.

Under hypoxia, GDH1 undergoes simultaneous acetylation at K503 and K527, which regulate GDH1 enzyme activity and target the EGLN1/HIF1 α complex, respectively. Lysine acetylation modifies enzyme activity, protein stability, and protein–protein interactions, among other effects (Choudhary et al, 2014). Hypoxia-induced GDH1 acetylation at K503 likely confers resistance to α KG feedback inhibition of GDH1, after which GDH1 can use α KG as a substrate to produce glutamate. The direction of the reaction will be determined when the concentrations of the substrate and product are no longer changed by the enzyme. A reversible reaction would occur if the accumulation of the product or the affinity of the enzyme to the product exhibits a significant increase. We previously reported that PGK1 phosphorylation caused a reversible reaction upon the stimulation of resident tissue macrophages secreting IL-6 (Zhang et al, 2018).

To ascertain the effect of the hypoxia-induced interaction between GDH1 and EGLN1 and of the decreased GDH1 α KG production activity on EGLN1 activity, we performed a series of experiments, as shown in Fig 5F–L. We first determined EGLN1 activity in cells with different genetic manipulations and used an *in vitro* assay in which different GDH1 mutants were incubated with EGLN1, and the results preliminarily linked GDH1 K503 and K527 acetylation to EGLN1 activity. Next, we applied both a radiometric ¹⁴C- α KG-EGLN1 binding assay and IP-LC/MS determination to identify the relative quantity of EGLN1 binding to α KG. Taken together, the data showed that a reverse GDH1 enzyme reaction occurred upon hypoxia and exhausted α KG around EGLN1 or impaired the affinity of EGLN1 for α KG.

p300 has been reported to positively regulate HIF1 α protein stability (Geng et al, 2012), and MUC1 has been shown to physically interact with HIF1 α and p300 to stabilize HIF1 α at the protein level

(Chaika *et al*, 2012). Consistently, we confirmed that p300 acetylated GDH1 under hypoxia and linked p300 to EGLN1 activity and HIF1 α stability. Moreover, HIF1 α significantly promoted the interaction between GDH1 and p300, and upregulated GDH1 acetylation. The initiation of GDH1 acetylation primarily promoted HIF1 α stabilization, which in turn promoted the interaction between GDH1 and p300, forming a positive cycle for fast accumulation of HIF1 α and a rapid response to hypoxic stress. This should be an important positive feedback loop which allows tumor cells to survive when facing hypoxia.

Although metabolic reprogramming is a hallmark of tumorigenesis and progression, little is known about the metabolic enzymes and oncometabolites that regulate CRC resistance to hypoxia and facilitate survival, and very few metabolic enzymes or molecules have been identified as potential biomarkers *in situ* (Sullivan *et al*, 2016). In this study, GDH1 acetylation at K527 facilitated GDH1 anchoring of EGLN1/HIF1 α , while GDH1 acetylation at K503 drove GDH1 to use α KG as a substrate to produce glutamate, the progression of which reduced the concentration of α KG around/in the EGLN1/HIF1 α complex or impaired the capacity of EGLN1 to bind α KG, both of which in turn stabilized HIF1 α . Therefore, the hypoxia-modulated acetylation of GDH1 at K503 and K527 is a potential biomarker of CRC progression, and the GDH1/EGLN1 axis is a potential target for CRC treatment (Fig 7M).

Materials and Methods

Patient specimens

Tumors and adjacent colorectal tissues were obtained from patients with CRC who underwent surgery or biopsy at The First Affiliated Hospital and The Third Affiliated Hospital of Sun Yat-sen University between 2012/08 and 2017/03. The patients had not received any chemotherapies or other treatments before surgery treatment or diagnosis at the hospital, harboring high or low AJCC stage level. The clinicopathological information was supplied in Tables EV1–EV4. The study protocol was approved by the Ethics Committee of Sun Yat-sen University (Guangzhou, China, ethics approval: #fahsysu-038). Written informed consent was obtained from all participants in this study. All the research was carried out in accordance with the provisions of the Declaration of Helsinki of 1975 and the Department of Health and Human Services Belmont Report.

IHC analysis

Tissue sections from paraffin-embedded human CRC tissues were stained with antibodies as indicated. We quantitatively scored the tissue sections according to the percentage of positive cells and the staining intensity. We rated the intensity of staining on a scale of 0–3: 0, negative; 1, weak; 2, moderate; and 3, strong. We assigned the following proportion scores: X indicates the percentage of the tumor cells that were stained ($0 \leq [X1 + X2 + X3] \leq 10$), where X3 indicates strong staining, X2 moderate staining and X1 weak staining. The score (H-score) was obtained using the following formula: $3 \times X1 + 2 \times X2 + 1 \times X3$, yielding scores ranging from 0 to 10. Scores were compared with overall survival, defined as the time from the date of diagnosis to death or the last known date of follow-up. The use of

human CRC specimens was approved by the IRB at Sun Yat-sen University Guangzhou Cancer Center and complied with all relevant ethical regulations. Informed consent was obtained from all patients.

AOM/DSS-induced colitis-associated colon cancer model

All mice were maintained under a 12-h light/dark cycle with free access to water and standard mouse chow in a specific-pathogen-free (SPF) facility, receiving humane care. All experimental procedures were performed in compliance with the Guide for the Care and Use of Laboratory Animals and approved by the Institutional Animal Care and Use Committee (IACUC) in Guangzhou University (Guangzhou, China, ethics approval: #gzhu2018039).

In the present study, the effect of AOM injection and DSS dietary administration was evaluated in GDH1^{IEC-/-} mice and control wild-type mice in C57BL/6 background. On Day 0, mice were given a single intraperitoneal injection of AOM (10 mg/kg body weight) at the age of 7 weeks old. Seven days after the AOM injection, the animals received 2% DSS (w/v) in the drinking water for 7 days, and then, drinking water alone was supplied for 7 days. The DSS-to-water cycle was repeated a total of three times. All animals were sacrificed on Day 80. At the time of sacrifice, a complete necropsy was performed on all mice. Histopathological examination was performed on paraffin-embedded sections after hematoxylin and eosin (H&E) staining.

Plasmids

pCDH-GDH1 and pColdI-His-GDH1 were constructed in a previous study (Wang *et al*, 2019a), as was pCDH-p300 (Wang *et al*, 2017). PCR-amplified HIF1 α was cloned into pCDH-GDH1. K503R/Q and K527R/Q mutations were generated using a QuickChange site-directed mutagenesis kit (Stratagene, La Jolla, CA, USA).

The pGIPZ control and pGIPZ GDH1 shRNA were generated as previously described (Wang *et al*, 2019a). The HIF1 α reporter plasmid was generated using the sequences cloned into the pGL3-TA promoter, and the sequence is listed in a previous report (Wang *et al*, 2019a).

Cell culture, transfection and designed antibody

Human CRC HCT116 and SW480 cell lines were purchased from American Type Culture Collection (ATCC). The cell lines were authenticated by STR-profiling and tested for mycoplasma contamination to ensure that they were mycoplasma-free. To induce hypoxic stress, the cells were cultured in a hypoxia incubator chamber (STEMCELL Technologies Inc., #27310).

Colorectal cells were transfected with small interfering RNAs (siRNAs, 50 nM) against human dehydrogenase and acetyltransferase-coding genes using MAX siRNA transfection reagent (Thermo Scientific Dharmacon Inc., USA), while nonspecific siRNA (siNC) was used as a negative control. All siRNAs were purchased from GenePharma Technology (Shanghai, China). siRNA sequences were listed in Appendix Table S1.

Antibodies against GDH1 acetylation at K503, K527, or K503/527 were custom designed and constructed by ABclonal Technology (Wuhan, China). Briefly, the acetyl-peptides AcK503-GDH1 (ISGA-SE_{Ac}KDIVHSG), AcK527-GDH1 (IMRTAM_{Ac}KYNLGL) and their respective control peptides without acetyl groups were first

synthesized. Then, New Zealand White (NZW) rabbits were immunized by intradermal injection of 500 μ g of indicated polypeptides which were mixed with Freund's adjuvant to 2 ml volume. This process was repeated three times, and the dose was reduced to half in the fourth time. Serum samples were taken to test the titers of indicated antibodies at 2 weeks after the fourth immunization. The antibodies were purified and obtained by affinity chromatography.

Quantitative RT-PCR (qRT-PCR)

Total RNA was extracted with an RNA high-purity total RNA rapid extraction kit (QIAGEN). cDNA was prepared using a GoScript reverse transcription system (Promega). qRT-PCR was performed using SYBR PCR premixture (Promega) and an ABI 7500 fast system under the following conditions: 5 min at 95°C followed by 38 cycles at 95°C for 30 s, 60°C for 40 s, and 72°C for 1 min. Data were normalized to the expression of the control gene (β -actin) for each experiment. Data are presented as the mean \pm SD of three independent experiments. The sequences of the primer pairs used for qRT-PCR were listed in Appendix Table S2.

Western blotting and antibodies

Western blot analysis was performed using standard protocols. An anti- β -actin (Merck, CAS: ABT264) antibody was used as a control for whole-cell lysates. Endogenous antibodies including HIF1 α (Clone number: D1S7W, CAS: #36169), HIF2 α (Clone number: E2N9W, CAS: #57921), EGLN1 (Clone number: D31E11, CAS: #4835), COX4 (Clone number: 3E11, CAS: #4850), p300 (Clone number: D8Z4E, CAS: #86377), AMPK (Clone number: D63G4, CAS: #5832), and Phospho-AMPK (Clone number: 40H9, CAS: #2535), GDH1 (Clone number: D9F7P, CAS: #12793), LaminB (Clone number: D9V6H, CAS: #13435), BCAT1 (Clone number: D4V2T, CAS: #16431), BCAT2 (Clone number: D8K3O, CAS: #79764), GOT1 (Clone number: E4A4O, CAS: #34423), GOT2 (CAS: #71692), GPT (CAS: AV45710) were purchased from Cell Signaling Technology. Antibodies including His-tag (Clone number: HIS.H8, CAS: ab18184), Pan-Methyl-Lysine (CAS: ab7315), Phospho-Ser/Thr (CAS: ab117253), Phospho-Tyrosine (Clone number: EPR16871, CAS: ab179530) were purchased from Abcam. Antibody IDH1/2 (CAS: sc-373816) was purchased from Santa Cruze. The dilution of these primary antibodies was 1:1,000. Tag antibodies against FLAG (CAS: AE005) or HA (CAS: A0208) and β -Tubulin (CAS: AC008) antibody were purchased from Abclonal (Wuhan, China) and used at a dilution of 1:5,000. IP and IB analyses were performed with the indicated antibodies.

Cell viability assay

HCT116 or SW480 cells with or without genetic modifications were plated in DMEM (10% FBS) under hypoxia or normoxia for the indicated times. Cells were collected at the indicated time points, and cell viability was determined by trypan blue staining.

PI/Annexin V

We measured the percentage of apoptotic cells under hypoxic stress as previously described (Shao *et al*, 2019).

Mass spectrometry analysis of GDH1-interacting proteins and GDH1 acetylation

GDH1-FLAG and its interacting proteins was enriched by immunoprecipitation with an antibody against the Flag tag. The proteins were eluted and separated using SDS-PAGE followed by Coomassie blue staining. The gel lane was dissected and subjected to in-gel digestion. Briefly, the gel was chopped into 1 mm³ pieces and decoloured using 50 mM NH₄HCO₃ in 30% ACN under oscillation. Then, the gel was subjected to vacuum freeze lyophilization and alkylated using 10 mM TCEP+ 50 mM CAA in 50 mM NH₄HCO₃ at 95°C for 5 min. The supernatant was removed, and the gel was again subjected to vacuum freeze lyophilization. Then, the gel was treated with trypsin (20 ng/ μ l in 50 mM NH₄HCO₃) and incubated at 37°C for 16 h. The peptides were extracted three times in an ultrasonic water bath by 0.1% TFA in 90% ACN. The resulting peptides were subjected to vacuum freeze lyophilization, purified using C18 stage tips and then analyzed via liquid chromatography-tandem mass spectrometry (LC-MS/MS). Peptides were loaded and separated on a homemade microtip C18 column (ReproSil-Pur C18-AQ, 3 μ m, 75 μ m \times 250 mm) on a nanoflow HPLC Easy-nLC 1000 system (buffer A, 0.1% FA in H₂O; buffer B, 0.1% FA in 100% ACN; Thermo Fisher Scientific). The LC gradient was set as follows: 2–4% B for 1 min; 4–30% B for 47 min; 30–45% B for 5 min; 45–90% B for 1 min; and 90% B for 6 min. MS data were collected via data-dependent acquisition in the profile mode on a Q Exactive mass spectrometer set as follows: MS1 resolution, 70,000 @ m/z 200; mass range, 300–1,600 m/z ; AGC Target, 3e6; maximum IT, 50 ms; topN, 10. MS2 resolution, 17,500 @ m/z 200; normalized collision energy (NCE), 27%; isolation width (m/z), 1.6 m/z ; AGC Target, 1e5; maximum IT, 120 ms; charge states include 2–5; dynamic exclusion, 30 s. The mass spectrometric data were analyzed using Proteome Discoverer 2.3 against the human Swiss-Prot database with carbamidomethyl cysteine set as a fixed modification and oxidized methionine, protein N-term acetylation and lysine acetylation set as variable modifications.

Lysine-acetylated GDH1 expression and purification

To obtain site-directed GDH1-AcK, we constructed pET22b-GDH1 encoding GDH1 with a C-terminal 6 \times His tag. We cotransformed *E. coli* BL21 (DE3) cells with pAckRS and pET22b-GDH1 with a C-terminal 6 \times His tag. As described previously (Neumann *et al*, 2008), GDH1-AcKs were overexpressed in *E. coli* BL21 (DE3) following the addition of Ara and IPTG in the presence of ampicillin, chloramphenicol, 10 mM NAM and AcK. GDH1-AcKs were purified by Ni-NTA affinity chromatography, followed by gel-filtration chromatography with a Superdex 75. The purity of the preparations was assessed by SDS-PAGE, and the protein concentration was determined using a Bradford protein assay kit.

Measurement of reversible GDH1 activity and GDH1 enzyme kinetics

GDH1 activity associated with α KG production was measured at room temperature. GDH1 was immunoprecipitated from the lysates of CRC cells or purified from *E. coli* and subjected to GDH1 enzymatic activity assays in reaction buffer containing 100 mM Tris (pH

8.0), 50 mM L-Glu, and 1 mM NAD⁺. The change in absorbance at 340 nm due to an increase in NADH was measured using a BioTek Synergy Neo Multi-Mode Plate Reader (BioTek, USA).

GDH1 activity associated with Glu production was measured at room temperature in reaction buffer containing 100 mM Tris (pH 8.0), 10 mM α KG, 5 mM NADH, and 500 μ M NH₄Cl. The change in absorbance at 340 nm due to a decrease in NADH was measured using a BioTek Synergy Neo Multi-Mode Plate Reader (BioTek, USA).

The continuous change in absorbance at 340 nm due to an increase or decrease in NADH was used to calculate the V_{max} of α KG or Glu, and the *K_m* was determined by nonlinear regression analysis, which was performed using Prism 7 (GraphPad).

Measurement of α KG

The indicated cells were seeded into six-well plates, then collected and lysed, and the lysate was examined using an α KG Assay Kit (Abcam, α KG Assay kit (colorimetric), CA, USA) according to the manufacturer's instructions.

Luciferase reporter assay

Transcriptional activation of HIF1 α in HCT116 cells was measured as previously described (Wang *et al.*, 2017). Relative levels of luciferase activity were normalized to the levels in untreated HCT116 cells expressing control vector and then normalized to the levels of luciferase activity induced by the Renilla control plasmid.

HIF peptide hydroxylation assay for assessing EGLN1 activity

An N-terminally biotinylated peptide corresponding to HIF1 residues 556–575 (DLDLEALAPYI PADDDFQLR) was synthesized by changing two methionines (M) to alanine (A). Equal amounts of HA-EGLN1 protein (10 nM) in HA beads were purified from the indicated HCT116 cells under hypoxia and incubated with the above peptide (100 nM) for 2 h in PHA buffer containing FeCl₂ (100 μ M), ascorbate (2 mM), and α KG (50 μ M). The HA agarose beads were washed three times with NETN (20 mM Tris–HCl [pH 8.0], 100 mM NaCl, 1 mM EDTA, 0.5% NP-40), and peptide hydroxylation was determined by LC–MS.

To measure GDH1 activity using α KG as a substrate and the consequence of α KG exhaustion in EGLN1, we first incubated His-GDH1 (including WT or mutant) with GST-EGLN1 (in the GST beads) in the adjusted buffer, changing 10 mM α KG to 500 μ M (called high α KG) or 80 μ M (called low α KG, which is likely close to the cytoplasmic α KG level under normal oxygen conditions) α KG. Then, EGLN1 was precold washed twice and incubated with HIF1 α to assess EGLN1 activity.

Measurement of EGLN1-bound α KG

To assess EGLN1-bound α KG, we first developed a radiometric ¹⁴C- α KG-EGLN1 binding assay. In detail, bead-bound HA-EGLN1 purified from the indicated HCT116 cells under hypoxia was washed with Tris-buffered saline (TBS) buffer (50 mM Tris, 150 mM NaCl [pH 7.5]), followed by incubation with 0.2 mCi ¹⁴C- α KG for 30 min in TBS buffer. The beads were then washed with TBS buffer

containing 1% NP-40. The bead-bound EGLN1 protein was eluted with 10 mg of HA peptides, and radioactivity was detected by liquid scintillation counting. We also developed another method for testing EGLN1-bound α KG using LC–MS. In detail, we enriched HA-EGLN1 from the indicated HCT116 cells under hypoxia and incubated HA-EGLN1 in TBS buffer containing 100 μ M α KG. HA-EGLN1 beads were quickly washed with TBS buffer containing 1% NP-40 but not α KG. Then, HA-EGLN1 was digested using protease to release α KG from the EGLN1 protein, and the α KG quantity was measured via liquid chromatography–mass spectrometry (LC–MS). The above results were normalized based on the total protein concentration in each sample.

Subcellular fractionation analyses

HCT116 cells were harvested and washed three times with cold PBS. Cytosolic or mitochondrial fractions were prepared using a Nuclear/Cytosol Fraction Kit (Active Motif).

Isothermal titration calorimetry

Thermodynamic parameters of the binding of GDH1 WT, K503R, or K503Q to Glu or α KG were measured by isothermal titration calorimetry (ITC) assays using an ITC200 Microcalorimeter (MicroCal) at 25°C. GDH1 was expressed in *E. coli* and purified via His tag affinity purification. In all experiments, the initial injection of 0.5 ml of Glu or α KG solution was discarded to eliminate the effect of titrant diffusion across the syringe tip during the equilibration process, and each dataset consisted of 20 injections of 2 ml each of 1 mM Glu or α KG into the sample cell containing 250 ml of 0.05 mM GDH1. The heat of dilution was negligible in all cases. The binding constant and other thermodynamic parameters were determined by fitting the integrated titration data using the single binding site model via the nonlinear least-squares method, which was implemented in MicroCal Origin software (version 7.0).

In vitro acetyltransferase activity assay

FLAG-tagged p300 was purified from HCT116 cells and eluted with the FLAG peptide. p300 was quantified as 50 ng/ μ l, and we added GDH1 to the p300 acetyltransferase activity reaction system according to the manufacturer's instructions. The acetyltransferase activity was measured using a kit (ab204536).

Subcutaneous xenograft model

All mice were maintained under a 12-h light/dark cycle with free access to water and standard mouse chow in a specific-pathogen-free (SPF) facility, receiving humane care. All experimental procedures were performed in compliance with the Guide for the Care and Use of Laboratory Animals and approved by the Institutional Animal Care and Use Committee (IACUC) in Guangzhou University (Guangzhou, China, ethics approval: #gzhu2018039).

Briefly, 2×10^6 HCT116-derived stable cells were subcutaneously injected into the left dorsal region of randomized 6-week-old male athymic nude mice. After inoculation for 28 days, the mice were euthanized, and the tumors were dissected. Differences in the weight of xenograft tumors were statistically analyzed.

Statistical analysis

All results are presented as the mean \pm standard deviation (SD), unless stated otherwise. Statistical analyses were performed using two tailed Student's *t*-test for two groups comparison, one-way or two-way analysis of variance (ANOVA) for multiple comparisons on GraphPad Prism version 8.3 (GraphPad Software, Inc.). About clinical patients, Mann–Whitney *U*-test was used for two groups comparison, Pearson's correlation analysis was used to calculate the regression and correlation, log-rank test was used to assess the patient survival curve. $P < 0.05$ was considered statistically significant. No statistical methods were applied to pre-evaluate sample size. The sample size was determined based on our experiences and similar with reported literature for specific experiments. No data were excluded from the analyses. All experiments were performed with at least three biologically independent samples or three biologically independent experiments. *n* values indicated biologically independent samples and experiments. Except the IHC scoring, the investigators were not blinded to allocation during experiments and outcome assessment for consistent of experimental procedures. For *in vivo* and *in vitro* assays, groups were randomly allocated.

Data availability

This study contains no data amenable to large-scale repository deposition.

Expanded View for this article is available [online](#).

Acknowledgements

This work was granted by the National Natural Science Foundation of China (92053113) and mainly supported by the Guangdong Basic and Applied Basic Research Foundation (2021B1515020016). In addition, we thanked a lot for the substantial support offered by the molecular biology platform at Precise Genome Engineering Center of Guangzhou University.

Author contributions

Xiongjun Wang: Resources; supervision; funding acquisition; writing – original draft; project administration; writing – review and editing. **Kunhua Hu:** Conceptualization; data curation; formal analysis; validation; investigation; methodology. **Yufeng Ding:** Resources; formal analysis; investigation; project administration; writing – review and editing. **Hongwen Zhu:** Data curation; software; formal analysis; validation; investigation; visualization; methodology. **Xiaoqian Jing:** Resources; formal analysis; validation; investigation; visualization. **Weiling He:** Resources; methodology. **Hua Yu:** Resources; formal analysis; supervision; validation; investigation; methodology; project administration.

Disclosure and competing interests statement

The authors declare that they have no conflict of interest.

References

Bögürcü N, Seidel S, Garvalov BK, Acker T (2018) Analysis of hypoxia and the hypoxic response in tumor xenografts. *Methods Mol Biol* 1742: 283–300

- Brahimi-Horn MC, Chiche J, Pouyssegur J (2007) Hypoxia and cancer. *J Mol Med (Berl)* 85: 1301–1307
- Chaika NV, Gebregiorgis T, Lewallen ME, Purohit V, Radhakrishnan P, Liu X, Zhang B, Mehla K, Brown RB, Caffrey T et al (2012) MUC1 mucin stabilizes and activates hypoxia-inducible factor 1 alpha to regulate metabolism in pancreatic cancer. *Proc Natl Acad Sci USA* 109: 13787–13792
- Choudhary C, Weinert BT, Nishida Y, Verdin E, Mann M (2014) The growing landscape of lysine acetylation links metabolism and cell signalling. *Nat Rev Mol Cell Biol* 15: 536–550
- De Robertis M, Massi E, Poeta ML, Carotti S, Morini S, Cecchetelli L, Signori E, Fazio VM (2011) The AOM/DSS murine model for the study of colon carcinogenesis: from pathways to diagnosis and therapy studies. *J Carcinog* 10: 9
- Geng H, Liu Q, Xue C, David LL, Beer TM, Thomas GV, Dai MS, Qian DZ (2012) HIF1 α protein stability is increased by acetylation at lysine 709. *J Biol Chem* 287: 35496–35505
- Hanahan D, Weinberg RA (2011) Hallmarks of cancer: the next generation. *Cell* 144: 646–674
- Jin L, Li D, Alesi GN, Fan J, Kang HB, Lu Z, Boggon TJ, Jin P, Yi H, Wright ER et al (2015) Glutamate dehydrogenase 1 signals through antioxidant glutathione peroxidase 1 to regulate redox homeostasis and tumor growth. *Cancer Cell* 27: 257–270
- Kaelin WG, Ratcliffe PJ (2008) Oxygen sensing by metazoans: the central role of the HIF hydroxylase pathway. *Mol Cell* 30: 393–402
- Ke Q, Costa M (2006) Hypoxia-inducible factor-1 (HIF-1). *Mol Pharmacol* 70: 1469–1480
- Koivunen P, Lee S, Duncan CG, Lopez G, Lu G, Ramkissoon S, Losman JA, Joensuu P, Bergmann U, Gross S et al (2012) Transformation by the (R)-enantiomer of 2-hydroxyglutarate linked to EGLN activation. *Nature* 483: 484–488
- Lorenzo FR, Huff C, Myllymäki M, Olenchock B, Swierczek S, Tashi T, Gordeuk V, Wuren T, Ri-Li G, McClain DA et al (2014) A genetic mechanism for Tibetan high-altitude adaptation. *Nat Genet* 46: 951–956
- Luo F, Liu X, Yan N, Li S, Cao G, Cheng Q, Xia Q, Wang H (2006) Hypoxia-inducible transcription factor-1alpha promotes hypoxia-induced A549 apoptosis via a mechanism that involves the glycolysis pathway. *BMC Cancer* 6: 26
- Neumann H, Peak-Chew SY, Chin JW (2008) Genetically encoding N(epsilon)-acetyllysine in recombinant proteins. *Nat Chem Biol* 4: 232–234
- Raffel S, Falcone M, Kneisel N, Hansson J, Wang W, Lutz C, Bullinger L, Poschet G, Nonnenmacher Y, Barnert A et al (2017) BCAT1 restricts α KG levels in AML stem cells leading to IDHmut-like DNA hypermethylation. *Nature* 551: 384–388
- Semenza GL (2003) Targeting HIF-1 for cancer therapy. *Nat Rev Cancer* 3: 721–732
- Shao J, Lu J, Zhu W, Yu H, Jing X, Wang YL, Wang X, Wang XJ (2019) Derepression of LOXL4 inhibits liver cancer growth by reactivating compromised p53. *Cell Death Differ* 26: 2237–2252
- Stillman TJ, Baker PJ, Britton KL, Rice DW (1993) Conformational flexibility in glutamate dehydrogenase. Role of water in substrate recognition and catalysis. *J Mol Biol* 234: 1131–1139
- Sullivan LB, Gui DY, Vander Heiden MG (2016) Altered metabolite levels in cancer: implications for tumour biology and cancer therapy. *Nat Rev Cancer* 16: 680–693
- Tarhonskaya H, Rydzik AM, Leung IK, Loik ND, Chan MC, Kawamura A, McCullagh JS, Claridge TD, Flashman E, Schofield CJ (2014) Non-enzymatic chemistry enables 2-hydroxyglutarate-mediated activation of 2-oxoglutarate oxygenases. *Nat Commun* 5: 3423

- Thaker AI, Shaker A, Rao MS, Ciorba MA (2012) Modeling colitis-associated cancer with azoxymethane (AOM) and dextran sulfate sodium (DSS). *J Vis Exp* <https://doi.org/10.3791/4100>
- Wang X, Qiao Y, Xiao M, Wang L, Chen J, Lv W, Xu L, Li Y, Wang Y, Tan MD et al (2017) Opposing roles of acetylation and phosphorylation in LIFR-dependent self-renewal growth signaling in mouse embryonic stem cells. *Cell Rep* 18: 933–946
- Wang X, Liu R, Qu X, Yu H, Chu H, Zhang Y, Zhu W, Wu X, Gao H, Tao B et al (2019a) α -ketoglutarate-activated NF- κ B signaling promotes compensatory glucose uptake and brain tumor development. *Mol Cell* 76: 148–162
- Wang Y, Bai C, Ruan Y, Liu M, Chu Q, Qiu L, Yang C, Li B (2019b) Coordinative metabolism of glutamine carbon and nitrogen in proliferating cancer cells under hypoxia. *Nat Commun* 10: 201
- Wapenaar H, Dekker FJ (2016) Histone acetyltransferases: challenges in targeting bi-substrate enzymes. *Clin Epigenetics* 8: 59
- Yang C, Sudderth J, Dang T, Bachoo RM, McDonald JG, DeBerardinis RJ (2009) Glioblastoma cells require glutamate dehydrogenase to survive impairments of glucose metabolism or Akt signaling. *Cancer Res* 69: 7986–7993
- Zhang Y, Yu G, Chu H, Wang X, Xiong L, Cai G, Liu R, Gao H, Tao B, Li W et al (2018) Macrophage-associated PGK1 phosphorylation promotes aerobic glycolysis and tumorigenesis. *Mol Cell* 71: 201–215
- Zhao S, Lin Y, Xu W, Jiang W, Zha Z, Wang P, Yu W, Li Z, Gong L, Peng Y et al (2009) Glioma-derived mutations in IDH1 dominantly inhibit IDH1 catalytic activity and induce HIF-1 α . *Science* 324: 261–265